Attosecond-level synchronisation of chip-integrated oscillators

Alexander E. Ulanov[1], Bastian Ruhnke[1], Thibault Wildi[1], Tobias Herr[1,2,*]

[1]Deutsches Elektronen-Synchrotron DESY, Notkestr. 85, 22607 Hamburg, Germany
[2]Physics Department, University of Hamburg UHH, Luruper Chaussee 149, 22761 Hamburg, Germany
[*]tobias.herr@desy.de

Attosecond science provides a window to the fastest processes in chemistry, materials science, and biology. Accessing this time scale requires precisely synchronised oscillators. In free-electron X-ray lasers, which also provide sub-atomic resolution, synchronisation must be achieved across hundreds of meters. Current approaches to synchronisation based on mode-locked lasers deliver this level of performance but complexity, cost and size hinder their deployment in facility-wide multi-node networks. Here, we demonstrate attosecond-level synchronisation of two chip-integrated photonic oscillators (microcombs) separated by 100 m of fibre. A pair of continuous-wave lasers establishes a time reference that is delivered over fibre, and on-chip Kerr-nonlinear synchronisation results in an integrated relative timing jitter of the microcombs below 400 as (1 kHz to 1 MHz), without any active stabilisation. These results unlock precision timing at scale for large facilities and next-generation technologies such as disaggregated computing and quantum networks, and ultimately may lead to chip-integrated attosecond photonics.

The fastest processes in chemistry, material science, and biology are governed by dynamics of bound electrons and occur on an attosecond time scale[1–4]. Free-electron X-ray lasers[5–8] (XFELs) and high-intensity laser beam lines[9] promise access to this regime, combined with sub-atomic spatial resolution. To reach this goal, facility-wide synchronisation on femto- or even attosecond level must be achieved[10–13]. Currently, the most advanced synchronisation techniques rely on optical methods, leveraging in particular the fact that synchronisation signals can be distributed over long distances via low-loss optical fibre. Several methods exist: (i) Intensity modulation of a continuous-wave laser[14,15] permits synchronisation with ∼10 fs relative timing jitter[16]. (ii) Using ultrashort pulse trains from a mode-locked laser as timing markers[17], attosecond-level (< 1 fs) relative timing jitter over a multi-kilometre fibre link has been demonstrated[18]. (iii) Synchronisation of mode-locked laser-based frequency combs based on distributing one or two continuous-wave (cw) optical carriers[19], locally generating low-noise radio-/microwave signals via optical frequency division (OFD)[20]. With actively stabilised fibre links frequency dissemination is possible[15,21], reaching a relative precision of 10^{-19} over almost 1000 km[22]. However, the complexity of current systems, often requiring actively stabilised table-top frequency combs, makes it challenging to deploy current synchronisation techniques across large, multi-node networks.

Microcombs provide a compact, low-cost, and scalable frequency comb platform, that can be integrated on photonic chips and potentially deployed in large networks[23–25]. They are generated via nonlinear optical frequency conversion in a microresonator pumped by a cw pump laser[26], enabling femtosecond pulses[27] with repetition rate from 10 GHz to 1 THz, and low-noise signal synthesis[28–31]. When a second (usually weaker) cw laser is injected into the microresonator, *Kerr-nonlinear synchronisation* locks the repetition rate to an integer fraction of the frequency difference between the cw lasers[32–38]. Recently this enabled the generation of ultra-pure microwaves[39] and also underpins synchronisation between microcombs or optical parametric oscillators within a microresonator[40–42] and between microresonators[43,44], including long-distance coherence transfer[45].

Here, we demonstrate precision synchronisation of two microcombs on separate photonic chips. We achieve this via Kerr-nonlinear synchronisation based on two cw lasers that are delivered to the microcombs via optical fibre (in our case 2 × 50 m). The frequency difference between both lasers defines a frequency reference to which the distributed microcombs synchronise without any active feedback loops, enabling precision timing across a fibre network (Fig. 1**a**). Using a frequency domain technique, we reveal a remarkably low relative timing jitter on the attosecond-level between the microcombs, well-below the microresonators' fundamental thermorefractive noise level, opening opportunities for precision synchronisation in large networks and chip-integrated attosecond science.

Results

The approach for synchronising the microcombs over fibre is as follows: A main pump laser of frequency ν_p generates the microcomb, which in the spectral domain contains discrete and equidistant frequencies $\nu_\mu = \nu_\mathrm{p} + \mu f_\mathrm{rep}$ (μ is line

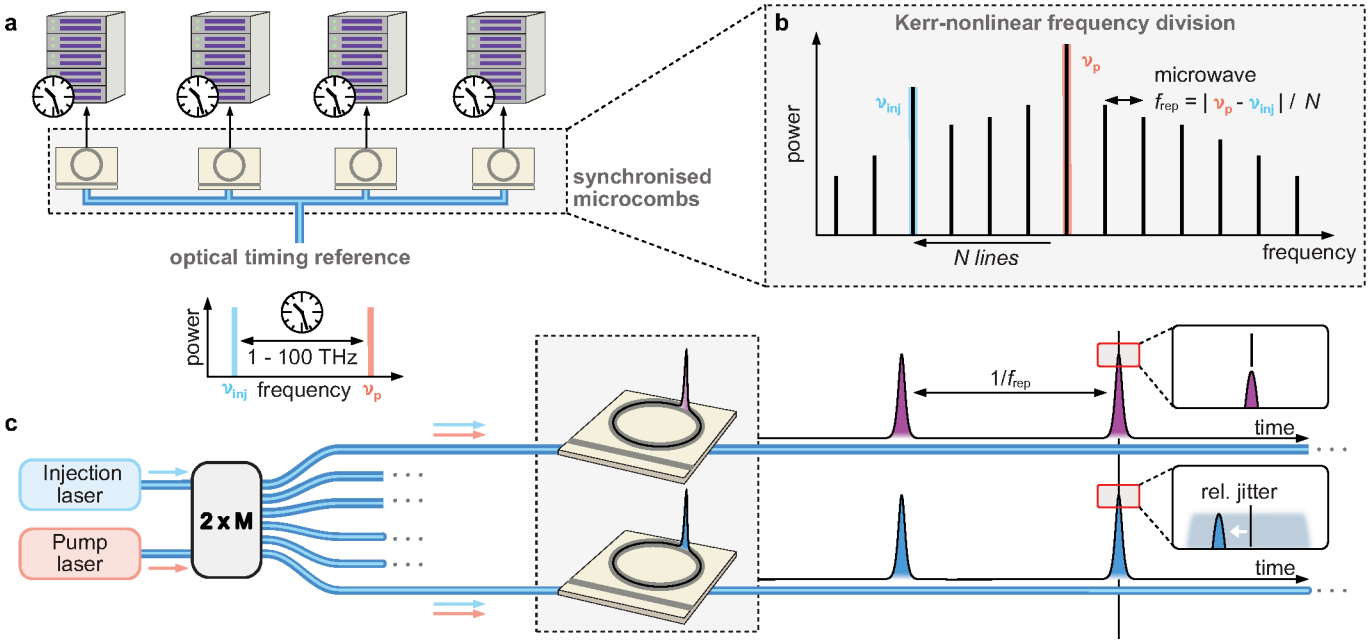

Figure 1 | Concept. **a**, Two laser frequencies (ν_p and ν_{inj}) define an optical timing reference that is distributed over fibre to different nodes in a timing network, where synchronised microcombs provide local precision timing. **b**, Both laser frequencies ν_p and ν_{inj} are part of the microcombs spectrum, whose discrete spectral components are spaced by $f_{rep} = |\nu_p - \nu_{inj}|/N$, where N is an integer. **b**, The two lasers with frequencies ν_p and ν_{inj} are combined and can then be distributed to M different microcombs via a $2 \times M$ fibre coupler. Both microcombs will emit pulses with the repetition rate f_{rep}, however, uncorrelated noise in both systems will lead to timing jitter.

index relative to the pump laser, f_{rep} is the pulse repetition rate). A second injection laser of frequency ν_{inj}, formally acting as a (weaker) second pump laser[37], enables Kerr-nonlinear synchronisation so that ν_p and ν_{inj} are both part of the microcomb spectra (see Fig. 1**b**). Effectively, this implements OFD where the frequency difference between the lasers is divided by an integer N into the microcomb microwave repetition rate $f_{rep} = |\nu_p - \nu_{inj}|/N$ (Fig. 1**b**). Both, pump and injection lasers, are combined and delivered over fibre to separate microcombs, implying that all comb frequencies and, in particular, the repetition rates of both combs are synchronised. However, both microcombs are still subject to uncorrelated noise inducing relative timing jitter, notably fundamental thermorefractive noise[46,47].

To investigate the synchronisation performance, we utilise a frequency domain technique, similar to the one developed for optical linewidth measurements in microcombs[48]. It is based on the elastic tape model describing the phase noise PSDs of the frequency comb lines[48,49]

$$S_\mu(f) = S_{\text{fix}}(f) + (\mu - \mu_{\text{fix}})^2 S_{\text{rep}}(f), \qquad (1)$$

where f is the noise frequency, S_{fix} represents the phase noise power spectral density (PSD) at the fix point at μ_{fix} (not necessarily an integer), and S_{rep} is the repetition rate phase noise PSD. In our case, we assume both microcombs have approximately the same μ_{fix}, which we will justify later. This implies that Eq. 1 can also describe the *relative* phase noise PSDs between the microcombs. Thus, considering all PSDs in Eq. 1 as relative noise quantities between the microcombs, we can retrieve the relative repetition rate phase noise $S^{\text{rel}}_{\text{rep}}(f)$ and relative timing jitter between the microcombs, based on measuring $S^{\text{rel}}_{\mu}(f)$ in dependence of μ and f.

The experimental setup for Kerr-nonlinear synchronisation and characterisation is shown in Fig. 2**a**. It consists of three main blocks: the pump source, the microcombs, and the characterisation stage. We use two free-running continuously-tunable cw lasers: The main pump laser ($\sim$ 1560 nm) is amplified to $\sim$ 630 mW of output power using an EDFA. The amplified spontaneous emission (ASE) is suppressed with a fibre Bragg grating (FBG) of $\sim$ 40 GHz bandwidth centred at the pump wavelength. The pump is then combined with the injection laser ($\sim$ 1618 nm), on a 50:50 fibre coupler. The two outputs of the coupler are used to drive two photonic crystal ring microresonators (PhCRs) on two different silicon nitride (Si_3N_4) integrated photonic chips. Both PhCRs have an intrinsic linewidth of $\sim$ 50 MHz, a free-spectral range (FSR) of $\sim$ 300 GHz (ring radius $\sim$ 75 μm), and are critically coupled; the waveguide cross-section is $1.6 \times 0.8\ \mu m^2$. Each PhCR features a periodic corrugation pattern along the inner wall with a spatial period of $\sim$ 422 nm creating a mode-frequency splitting of the $\mu = 0$ resonance of $\sim$ 250 MHz, enabling deterministic excitation of single soliton microcombs[50,51]. Optical input-output coupling to the photonic chips is implemented using ultra-high-numerical-aperture fibres with index-matching gel to sup-

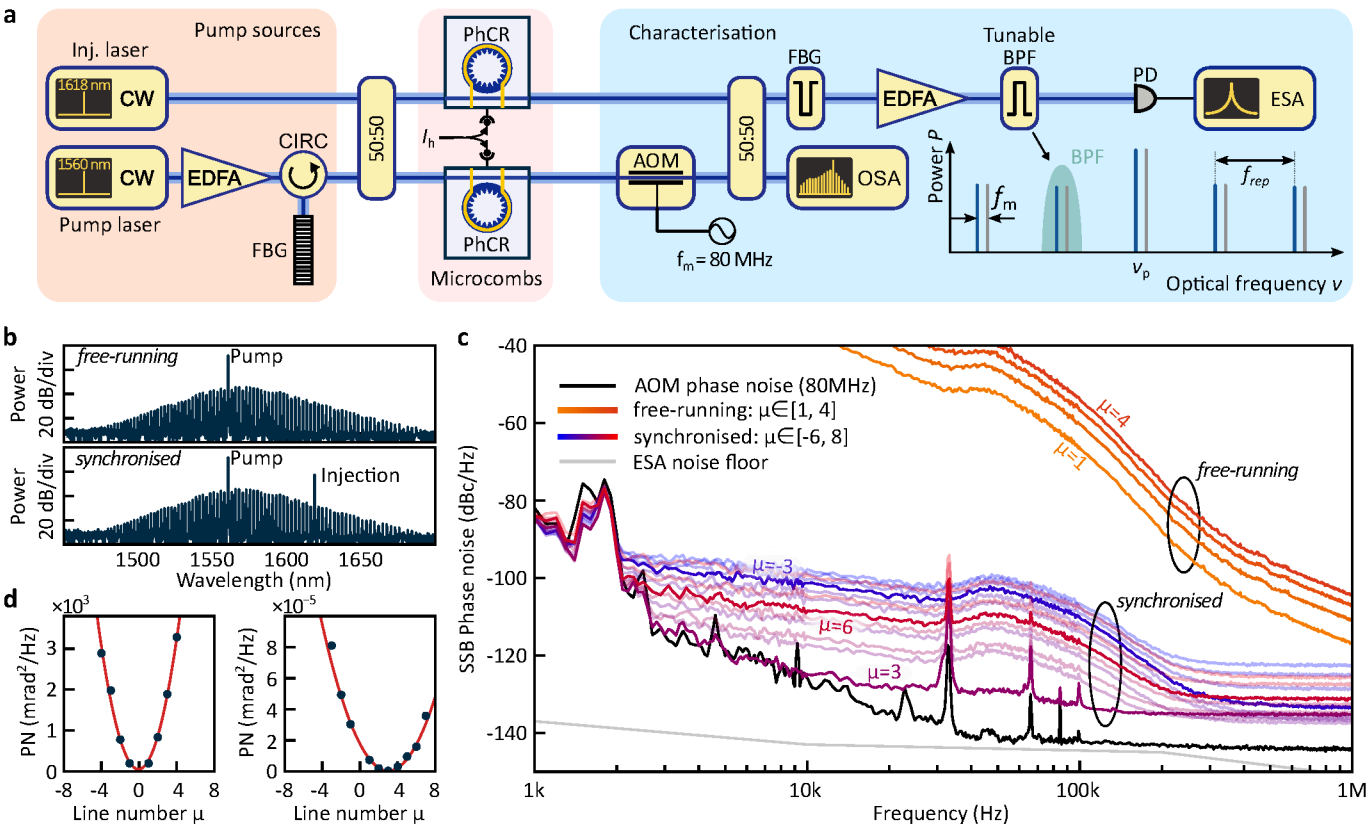

Figure 2 | Experimental approach. **a**, Schematic of the experimental setup. Two cw lasers (pump and injection) are combined on a 3 dB coupler and used to pump two identical photonic crystal resonators (PhCRs). An acousto-optic modulator (AOM) shifts the output of one comb by 80 MHz, after which both combs are recombined at a fibre coupler and amplified using an erbium-doped fibre amplifier (EDFA). A tunable bandpass filter (BPF) is used to select a single pair of comb lines (see inset). PD - photodiode, ESA - electrical spectrum analyser, FBG - fiber Bragg grating. **b**, Optical spectrum of two independent microcombs in the free-running (top, no injection) and synchronised (bottom, with injection) regimes. **c**, Single-sideband (SSB) phase-noise power spectral density (PSD) of the beatnotes between pairs of comb lines with index μ, measured in the free-running and synchronised states. The measurement is limited by the phase-noise of the AOM, which is retrieved from the beating between shifted and unshifted pump (black) and the ESA noise floor (gray). **d**, Phase-noise (PN) PSD at 10 kHz analysis frequency, extracted from the data in **c**, in the free-running (left) and synchronised (right) states. PN is shown using linear scaling ($\mathrm{mrad}^2/\mathrm{Hz}$).

press parasitic back-reflections, resulting in approximately 100 mW of on-chip pump power per chip. The microcombs with $f_{\mathrm{rep}} \approx 300$ GHz are initiated by adjusting the detuning of the $\mu = 0$ resonance with regard to the pump laser frequency ν_{p} via chip-integrated electric microheaters. To investigate the relative timing jitter between the two microcombs, one of them is shifted in frequency by 80 MHz via an acousto-optic modulator (AOM; see Fig. 2**a**), before they are recombined via a 50:50 fibre coupler. After rejecting the pump line with an FBG, we obtain ~ 2 mW of total optical power in each of the two output ports of the coupler. One output is amplified with a second EDFA to 200 mW and passed through a tunable fibre-coupled bandpass filter (implemented using a commercial waveshaper), which can either transmit the entire spectrum or select individual comb lines with ~ 25 GHz bandwidth. The filtered signal is detected on a low-noise photodiode and analysed using an electrical spectrum analyser (ESA). The second output is reserved for auxiliary measurements such as optical spectra or power detection.

First, we characterise the microcombs in the free-running regime (injection laser off), where both microcombs operate with a repetition rate difference of $\Delta f_{\mathrm{rep}} \approx 5$ MHz. Their combined optical spectra are shown in Fig. 2**b** (top panel). We sequentially center the bandpass filter on each pair of microcomb lines with $\mu \in [-4, 4]$ and measure with the ESA the single-sideband (SSB) phase noise $S_\mu^{\mathrm{rel}}(f)$ of the corresponding beatnote. The results, shown in Fig. 2**c**, indicate that the relative phase noise between comb lines increases with $|\mu|$, with the lowest noise observed at the ± 1 sidebands (for better visibility we only show the traces for $\mu = 1..4$). From these measurements, we extract the phase noise at a fixed offset (10 kHz) and plot it as a function of line number μ, revealing an almost ideal parabolic dependence on the mode number μ (see Fig. 2**d**). This is consistent with the elastic tape model, where both combs are independently 'breathing' around their common spectral fix point with $S_{\mathrm{rep}}(f)$. The fix point is here close to the pump laser at $\mu = 0$ and additional relative fix point noise $S_{\mathrm{fix}}^{\mathrm{rel}}(f)$ that would manifest

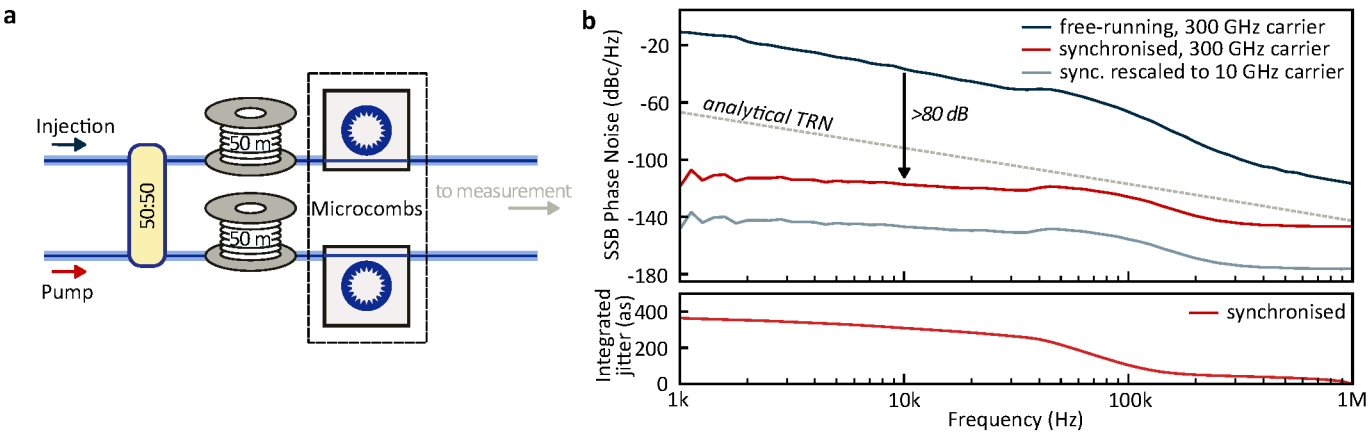

Figure 3 | Phase noise and timing jitter of synchronised microcombs. **a**, Experimental setup with 50 m of spooled single-mode fibre added in both arms before the chips. **b**, (top) Relative repetition rate single-sideband (SSB) phase-noise power spectral density in the free-running (dark blue) and synchronised (red) states at 300 GHz carrier. The dashed line indicates an analytic estimate[46] of the fundamental thermorefractive noise (TRN) for the 300 GHz microresonator, and the gray trace shows the relative repetition rate noise rescaled to 10 GHz carrier. (bottom) The corresponding integrated residual timing jitter in the synchronised state.

as a vertical offset of the parabola is negligible.

Next, we set Δf_{rep} close to zero. This is readily possible as it can be continuously tuned via the microheaters across multiple tens of megahertz, while maintaining microcomb operation. To trigger Kerr-nonlinear synchronisation, we switch on the injection laser, and tune it toward the $\mu' = 23$ comb lines (≈ 1618 nm). When sufficiently close to the comb lines, the injection laser enters the sideband injection-locking range $\delta_{\mathrm{lock}} \propto \mu'^2 \sqrt{P_{\mathrm{inj}} P_{\mu'}}$, where P_{inj} and $P_{\mu'}$ are the injected power and the power of the comb line μ', respectively[37]. In our case, the sideband injection locking range δ_{lock} exceeds 200 MHz, and the achievable locking bandwidth can be estimated to be of the same order[39]. Once locked, the μ' lines of both combs latch onto the injection laser, forcing their frequencies to coincide with the injection laser frequency, resulting in $\Delta f_{\mathrm{rep}} = 0$. All beatnotes between comb line pairs are now at the AOM frequency $f_m = 80$ MHz.

In this synchronised state, we again measure the RF beatnote SSB phase noise (see Fig. 2**c**) for comb sidebands $\mu \in [-6, 8]$, revealing a drastically reduced relative phase noise, indicating tight synchronization. Here, the injection laser plays two roles: (i) it provides a second frequency pin-point for both microcombs, which, through OFD, defines their repetition rates according to $f_{\mathrm{rep}} = |\nu_{\mathrm{p}} - \nu_{\mathrm{inj}}|/\mu'$ and forces $\Delta f_{\mathrm{rep}} = 0$; (ii) it suppresses absolute repetition rate phase noise via OFD[39]. As before, we use the measured data to compute the phase noise at a given offset frequency for each measured pair of comb lines and plot the results as a function of the line number (see Fig. 2**d**). The results again reveal a parabolic dependence, consistent with the elastic tape model, but this time with a shifted fix point μ_{fix}, that we assume is the same for both microcombs. This assumption is motivated by the fact that the PhCRs are of identical design and driven with nearly equal laser powers and justified by the fact that the data is well described by a single parabola. These observations confirm the validity of our approach.

Before proceeding with our analysis, we introduce 50 m of single-mode fibre (spooled) into both arms before the chips (see Fig. 3**a**) to emulate a realistic timing distribution scenario across 100 m distance. In this configuration, we repeat the measurement of the phase noise to obtain $S_{\mu}^{\mathrm{rel}}(f)$ in the free-running and synchronised regimes. To explicitly derive $S_{\mathrm{rep}}^{\mathrm{rel}}(f)$ (and the timing jitter), we fit the parabolic $S_{\mu}^{\mathrm{rel}}(f)$ at 60 points on the logarithmic f axis. Based on Eq. 1, we determine the phase noise PSD $S_{\mathrm{rep}}^{\mathrm{rel}}(f)$ of the 300 GHz repetition rate signal, as shown in Fig. 3**b** (top): Kerr-nonlinear synchronisation results in a striking reduction of the phase noise compared to the free-running case by more than eight orders of magnitude (80 dB) to well below the thermorefractive noise level. Notably, this performance is achieved without any active feedback loops, only relying on the Kerr-nonlinear synchronisation by the two free-running cw lasers. For comparison with other oscillators, Fig. 3**b** also shows the corresponding spectrum rescaled to a 10 GHz carrier frequency. In Fig. 3**b** (bottom) we plot the integrated relative timing jitter between both combs, which is below 380 attoseconds when integrated from 1 kHz to 1 MHz. This signifies attosecond-level synchronization of two chip-integrated photonic oscillators separated by 100 meters of optical fibre, opening a pathway to scalable precision synchronization in multi-node optical networks.

Conclusion

In conclusion, we demonstrate the first attosecond-level synchronisation of microcomb oscillators. The synchronisation is achieved by transmitting a main pump laser and a second injection laser over fibre to the two microcombs. Kerr-nonlinear synchronisation reduces the relative phase noise and timing jitter between both oscillators by more than 80 dB resulting in a remarkably low integrated rel-

ative timing jitter of less than 400 as. While in our case the lasers were free-running, they could be stabilized to a low noise reference cavity, or derived from a low-noise mode-locked laser, enabling precision synchronisation between complementary laser technologies. Moreover, while we use sources with $f_{\mathrm{rep}} = 300$ GHz, our results apply equally to systems with lower and directly detectable repetition rate, as well as normal dispersion switching wave combs[37,52]. These results could enable precision timing across large networks in attosecond experiments, radio-telescopes, geodesy, or in increasingly demanding and emerging technological applications such as data centres and large-scale computing facilities[53–55], quantum-secure communication and quantum-information[56–60]. Ultimately, our results may lead to chip-integrated attosecond photonics.

Funding. This project has received funding from the European Research Council (ERC) under the EU's Horizon 2020 research and innovation program (grant agreement No 853564), from the EU's Horizon 2020 research and innovation program (grant agreement No 101137000) and through the Helmholtz Young Investigators Group VH-NG-1404; the work was supported through the Maxwell computational resources operated at DESY.

References

1. Hentschel, M., Kienberger, R., Spielmann, C., Reider, G. A., Milosevic, N., Brabec, T., Corkum, P., Heinzmann, U., Drescher, M. & Krausz, F. Attosecond Metrology. *Nature* **414,** 509–513 (2001).
2. Drescher, M., Hentschel, M., Kienberger, R., Uiberacker, M., Yakovlev, V., Scrinzi, A., Westerwalbesloh, T., Kleineberg, U., Heinzmann, U. & Krausz, F. Time-Resolved Atomic Inner-Shell Spectroscopy. *Nature* **419,** 803–807 (2002).
3. Calegari, F., Ayuso, D., Trabattoni, A., Belshaw, L., De Camillis, S., Anumula, S., Frassetto, F., Poletto, L., Palacios, A., Decleva, P., Greenwood, J. B., Martín, F. & Nisoli, M. Ultrafast Electron Dynamics in Phenylalanine Initiated by Attosecond Pulses. *Science* **346,** 336–339 (2014).
4. Li, S., Lu, L., Bhattacharyya, S., Pearce, C., Li, K., Nienhuis, E. T., Doumy, G., Schaller, R. D., Moeller, S., Lin, M.-F., Dakovski, G., Hoffman, D. J., Garratt, D., Larsen, K. A., Koralek, J. D., Hampton, C. Y., Cesar, D., Duris, J., Zhang, Z., Sudar, N., Cryan, J. P., Marinelli, A., Li, X., Inhester, L., Santra, R. & Young, L. Attosecond-Pump Attosecond-Probe x-Ray Spectroscopy of Liquid Water. *Science* **383,** 1118–1122 (2024).
5. Emma, P., Akre, R., Arthur, J., Bionta, R., Bostedt, C., Bozek, J., Brachmann, A., Bucksbaum, P., Coffee, R., Decker, F.-J., Ding, Y., Dowell, D., Edstrom, S., Fisher, A., Frisch, J., Gilevich, S., Hastings, J., Hays, G., Hering, P., Huang, Z., Iverson, R., Loos, H., Messerschmidt, M., Miahnahri, A., Moeller, S., Nuhn, H.-D., Pile, G., Ratner, D., Rzepiela, J., Schultz, D., Smith, T., Stefan, P., Tompkins, H., Turner, J., Welch, J., White, W., Wu, J., Yocky, G. & Galayda, J. First Lasing and Operation of an Ångstrom-Wavelength Free-Electron Laser. *Nature Photonics* **4,** 641–647 (2010).
6. Allaria, E., Appio, R., Badano, L., Barletta, W. A., Bassanese, S., Biedron, S. G., Borga, A., Busetto, E., Castronovo, D., Cinquegrana, P., Cleva, S., Cocco, D., Cornacchia, M., Craievich, P., Cudin, I., D'Auria, G., Dal Forno, M., Danailov, M. B., De Monte, R., De Ninno, G., Delgiusto, P., Demidovich, A., Di Mitri, S., Diviacco, B., Fabris, A., Fabris, R., Fawley, W., Ferianis, M., Ferrari, E., Ferry, S., Froehlich, L., Furlan, P., Gaio, G., Gelmetti, F., Giannessi, L., Giannini, M., Gobessi, R., Ivanov, R., Karantzoulis, E., Lonza, M., Lutman, A., Mahieu, B., Milloch, M., Milton, S. V., Musardo, M., Nikolov, I., Noe, S., Parmigiani, F., Penco, G., Petronio, M., Pivetta, L., Predonzani, M., Rossi, F., Rumiz, L., Salom, A., Scafuri, C., Serpico, C., Sigalotti, P., Spampinati, S., Spezzani, C., Svandrlik, M., Svetina, C., Tazzari, S., Trovo, M., Umer, R., Vascotto, A., Veronese, M., Visintini, R., Zaccaria, M., Zangrando, D. & Zangrando, M. Highly Coherent and Stable Pulses from the FERMI Seeded Free-Electron Laser in the Extreme Ultraviolet. *Nature Photonics* **6,** 699–704 (2012).
7. Decking, W. *et al.* A MHz-repetition-rate Hard X-ray Free-Electron Laser Driven by a Superconducting Linear Accelerator. *Nature Photonics* **14,** 391–397 (2020).
8. Prat, E., Al Haddad, A., Arrell, C., Augustin, S., Boll, M., Bostedt, C., Calvi, M., Cavalieri, A. L., Craievich, P., Dax, A., Dijkstal, P., Ferrari, E., Follath, R., Ganter, R., Geng, Z., Hiller, N., Huppert, M., Ischebeck, R., Juranić, P., Kittel, C., Knopp, G., Malyzhenkov, A., Marcellini, F., Neppl, S., Reiche, S., Sammut, N., Schietinger, T., Schmidt, T., Schnorr, K., Trisorio, A., Vicario, C., Voulot, D., Wang, G. & Weilbach, T. An X-ray Free-Electron Laser with a Highly Configurable Undulator and Integrated Chicanes for Tailored Pulse Properties. *Nature Communications* **14,** 5069 (2023).
9. Kühn, S., Dumergue, M., Kahaly, S., Mondal, S., Füle, M., Csizmadia, T., Farkas, B., Major, B., Várallyay, Z., Cormier, E., Kalashnikov, M., Calegari, F., Devetta, M., Frassetto, F., Månsson, E., Poletto, L., Stagira, S., Vozzi, C., Nisoli, M., Rudawski, P., Maclot, S., Campi, F., Wikmark, H.,

Arnold, C. L., Heyl, C. M., Johnsson, P., L'Huillier, A., Lopez-Martens, R., Haessler, S., Bocoum, M., Boehle, F., Vernier, A., Iaquaniello, G., Skantzakis, E., Papadakis, N., Kalpouzos, C., Tzallas, P., Lépine, F., Charalambidis, D., Varjú, K., Osvay, K. & Sansone, G. The ELI-ALPS Facility: The next Generation of Attosecond Sources. *Journal of Physics B: Atomic, Molecular and Optical Physics* **50,** 132002 (2017).

10. Schulz, S., Grguraš, I., Behrens, C., Bromberger, H., Costello, J. T., Czwalinna, M. K., Felber, M., Hoffmann, M. C., Ilchen, M., Liu, H. Y., Mazza, T., Meyer, M., Pfeiffer, S., Prędki, P., Schefer, S., Schmidt, C., Wegner, U., Schlarb, H. & Cavalieri, A. L. Femtosecond All-Optical Synchronization of an X-ray Free-Electron Laser. *Nature Communications* **6,** 5938 (2015).

11. Hartmann, N., Hartmann, G., Heider, R., Wagner, M. S., Ilchen, M., Buck, J., Lindahl, A. O., Benko, C., Grünert, J., Krzywinski, J., Liu, J., Lutman, A. A., Marinelli, A., Maxwell, T., Miahnahri, A. A., Moeller, S. P., Planas, M., Robinson, J., Kazansky, A. K., Kabachnik, N. M., Viefhaus, J., Feurer, T., Kienberger, R., Coffee, R. N. & Helml, W. Attosecond Time–Energy Structure of X-ray Free-Electron Laser Pulses. *Nature Photonics* **12,** 215–220 (2018).

12. Xin, M., Şafak, K. & Kärtner, F. X. Ultra-Precise Timing and Synchronization for Large-Scale Scientific Instruments. *Optica* **5,** 1564–1578 (2018).

13. Sato, T., Letrun, R., Kirkwood, H. J., Liu, J., Vagovič, P., Mills, G., Kim, Y., Takem, C. M. S., Planas, M., Emons, M., Jezynski, T., Palmer, G., Lederer, M., Schulz, S., Mueller, J., Schlarb, H., Silenzi, A., Giovanetti, G., Parenti, A., Bergemann, M., Michelat, T., Szuba, J., Grünert, J., Chapman, H. N. & Mancuso, A. P. Femtosecond Timing Synchronization at Megahertz Repetition Rates for an X-Ray Free-Electron Laser. *Optica* **7,** 716–717 (2020).

14. Narbonneau, F., Lours, M., Bize, S., Clairon, A., Santarelli, G., Lopez, O., Daussy, C., Amy-Klein, A. & Chardonnet, C. High Resolution Frequency Standard Dissemination via Optical Fiber Metropolitan Network. *Review of Scientific Instruments* **77,** 064701 (2006).

15. Foreman, S. M., Holman, K. W., Hudson, D. D., Jones, D. J. & Ye, J. Remote Transfer of Ultrastable Frequency References via Fiber Networks. *Review of Scientific Instruments* **78,** 021101 (2007).

16. Wilcox, R., Byrd, J. M., Doolittle, L., Huang, G. & Staples, J. W. Stable Transmission of Radio Frequency Signals on Fiber Links Using Interferometric Delay Sensing. *Optics Letters* **34,** 3050–3052 (2009).

17. Hudson, D. D., Foreman, S. M., Cundiff, S. T. & Ye, J. Synchronization of Mode-Locked Femtosecond Lasers through a Fiber Link. *Optics Letters* **31,** 1951–1953 (2006).

18. Xin, M., Şafak, K., Peng, M. Y., Kalaydzhyan, A., Wang, W.-T., Mücke, O. D. & Kärtner, F. X. Attosecond Precision Multi-Kilometer Laser-Microwave Network. *Light: Science & Applications* **6,** e16187–e16187 (2017).

19. Coddington, I., Swann, W. C., Lorini, L., Bergquist, J. C., Le Coq, Y., Oates, C. W., Quraishi, Q., Feder, K. S., Nicholson, J. W., Westbrook, P. S., Diddams, S. A. & Newbury, N. R. Coherent Optical Link over Hundreds of Metres and Hundreds of Terahertz with Subfemtosecond Timing Jitter. *Nature Photonics* **1,** 283–287 (2007).

20. Fortier, T. M., Kirchner, M. S., Quinlan, F., Taylor, J., Bergquist, J. C., Rosenband, T., Lemke, N., Ludlow, A., Jiang, Y., Oates, C. W. & Diddams, S. A. Generation of Ultrastable Microwaves via Optical Frequency Division. *Nature Photonics* **5,** 425–429 (2011).

21. Lopez, O., Amy-Klein, A., Daussy, C., Chardonnet, C., Narbonneau, F., Lours, M. & Santarelli, G. 86-Km Optical Link with a Resolution of $2 \times 10\text{-}18$ for RF Frequency Transfer. *The European Physical Journal D* **48,** 35–41 (2008).

22. Predehl, K., Grosche, G., Raupach, S. M. F., Droste, S., Terra, O., Alnis, J., Legero, T., Hänsch, T. W., Udem, T., Holzwarth, R. & Schnatz, H. A 920-Kilometer Optical Fiber Link for Frequency Metrology at the 19th Decimal Place. *Science* **336,** 441–444 (2012).

23. Kippenberg, T. J., Gaeta, A. L., Lipson, M. & Gorodetsky, M. L. Dissipative Kerr Solitons in Optical Microresonators. *Science* **361,** eaan8083 (2018).

24. Pasquazi, A., Peccianti, M., Razzari, L., Moss, D. J., Coen, S., Erkintalo, M., Chembo, Y. K., Hansson, T., Wabnitz, S., Del'Haye, P., Xue, X., Weiner, A. M. & Morandotti, R. Micro-Combs: A Novel Generation of Optical Sources. *Physics Reports. Micro-Combs: A Novel Generation of Optical Sources* **729,** 1–81 (2018).

25. Gaeta, A. L., Lipson, M. & Kippenberg, T. J. Photonic-Chip-Based Frequency Combs. *Nature Photonics* **13,** 158–169 (2019).

26. Del'Haye, P., Schliesser, A., Arcizet, O., Wilken, T., Holzwarth, R. & Kippenberg, T. J. Optical Frequency Comb Generation from a Monolithic Microresonator. *Nature* **450,** 1214–1217 (2007).

27. Herr, T., Brasch, V., Jost, J. D., Wang, C. Y., Kondratiev, N. M., Gorodetsky, M. L. & Kippenberg, T. J. Temporal Solitons in Optical Microresonators. *Nature Photonics* **8,** 145–152 (2014).

28. Lucas, E., Brochard, P., Bouchand, R., Schilt, S., Südmeyer, T. & Kippenberg, T. J. Ultralow-Noise Photonic Microwave Synthesis Using a Soliton Microcomb-Based Transfer Oscillator. *Nature Communications* **11,** 374 (2020).

29. Kudelin, I., Groman, W., Ji, Q.-X., Guo, J., Kelleher, M. L., Lee, D., Nakamura, T., McLemore, C. A., Shirmohammadi, P., Hanifi, S., Cheng, H., Jin, N., Wu, L., Halladay, S., Luo, Y., Dai, Z., Jin, W., Bai, J., Liu, Y., Zhang, W., Xiang, C., Chang, L., Iltchenko, V., Miller, O., Matsko, A., Bowers, S. M., Rakich, P. T., Campbell, J. C., Bowers, J. E., Vahala, K. J., Quinlan, F. & Diddams, S. A. Photonic Chip-Based Low-Noise Microwave Oscillator. *Nature* **627,** 534–539 (2024).

30. Sun, S., Wang, B., Liu, K., Harrington, M. W., Tabatabaei, F., Liu, R., Wang, J., Hanifi, S., Morgan, J. S., Jahanbozorgi, M., Yang, Z., Bowers, S. M., Morton, P. A., Nelson, K. D., Beling, A., Blumenthal, D. J. & Yi, X. Integrated Optical Frequency Division for Microwave and mmWave Generation. *Nature* **627,** 540–545 (2024).

31. Zang, J., Briles, T. C., Morgan, J. S., Beling, A. & Papp, S. B. *Universal Electronic Synthesis by Microresonator-Soliton Photomixing* 2025. arXiv: `2505.08707 [physics]`.

32. Jang, J. K., Erkintalo, M., Coen, S. & Murdoch, S. G. Temporal Tweezing of Light through the Trapping and Manipulation of Temporal Cavity Solitons. *Nature Communications* **6,** 7370 (2015).

33. Taheri, H., Matsko, A. B. & Maleki, L. Optical Lattice Trap for Kerr Solitons. *The European Physical Journal D* **71,** 153 (2017).

34. Weng, W., Lucas, E., Lihachev, G., Lobanov, V. E., Guo, H., Gorodetsky, M. L. & Kippenberg, T. J. Spectral Purification of Microwave Signals with Disciplined Dissipative Kerr Solitons. *Physical Review Letters* **122,** 013902 (2019).

35. Brasch, V., Obrzud, E., Lecomte, S. & Herr, T. Nonlinear Filtering of an Optical Pulse Train Using Dissipative Kerr Solitons. *Optica* **6,** 1386 (2019).

36. Moille, G., Stone, J., Chojnacky, M., Shrestha, R., Javid, U. A., Menyuk, C. & Srinivasan, K. Kerr-Induced Synchronization of a Cavity Soliton to an Optical Reference. *Nature* **624,** 267–274 (2023).

37. Wildi, T., Ulanov, A., Englebert, N., Voumard, T. & Herr, T. Sideband Injection Locking in Microresonator Frequency Combs. *APL Photonics* **8,** 120801 (2023).

38. Lei, F., Sun, Y., Helgason, Ó. B., Ye, Z., Gao, Y., Karlsson, M., Andrekson, P. A. & Torres-Company, V. Self-Injection-Locked Optical Parametric Oscillator Based on Microcombs. *Optica* **11,** 420–426 (2024).

39. Sun, S., Harrington, M. W., Tabatabaei, F., Hanifi, S., Liu, K., Wang, J., Wang, B., Yang, Z., Liu, R., Morgan, J. S., Bowers, S. M., Morton, P. A., Nelson, K. D., Beling, A., Blumenthal, D. J. & Yi, X. Microcavity Kerr Optical Frequency Division with Integrated SiN Photonics. *Nature Photonics* **19,** 637–642 (2025).

40. Yang, Q.-F., Yi, X., Yang, K. Y. & Vahala, K. Counter-Propagating Solitons in Microresonators. *Nature Photonics* **11,** 560–564 (2017).

41. Zhang, S., Silver, J. M., Bi, T. & Del'Haye, P. Spectral Extension and Synchronization of Microcombs in a Single Microresonator. *Nature Communications* **11,** 6384 (2020).

42. Zhao, Y., Jang, J. K., Beals, G. J., McNulty, K. J., Ji, X., Okawachi, Y., Lipson, M. & Gaeta, A. L. All-Optical Frequency Division on-Chip Using a Single Laser. *Nature* **627,** 546–552 (2024).

43. Jang, J. K., Klenner, A., Ji, X., Okawachi, Y., Lipson, M. & Gaeta, A. L. Synchronization of Coupled Optical Microresonators. *Nature Photonics* **12,** 688–693 (2018).

44. Kim, B. Y., Jang, J. K., Okawachi, Y., Ji, X., Lipson, M. & Gaeta, A. L. Synchronization of Nonsolitonic Kerr Combs. *Science Advances* **7,** eabi4362 (2021).

45. Geng, Y., Zhou, H., Han, X., Cui, W., Zhang, Q., Liu, B., Deng, G., Zhou, Q. & Qiu, K. Coherent Optical Communications Using Coherence-Cloned Kerr Soliton Microcombs. *Nature Communications* **13,** 1070 (2022).

46. Kondratiev, N. M. & Gorodetsky, M. L. Thermorefractive Noise in Whispering Gallery Mode Microresonators: Analytical Results and Numerical Simulation. *Physics Letters A. Special Issue in Memory of Professor V.B. Braginsky* **382,** 2265–2268 (2018).

47. Huang, G., Lucas, E., Liu, J., Raja, A. S., Lihachev, G., Gorodetsky, M. L., Engelsen, N. J. & Kippenberg, T. J. Thermorefractive Noise in Silicon-Nitride Microresonators. *Physical Review A* **99,** 061801 (2019).

48. Lei, F., Ye, Z., Helgason, Ó. B., Fülöp, A., Girardi, M. & Torres-Company, V. Optical Linewidth of Soliton Microcombs. *Nature Communications* **13,** 3161 (2022).

49. Liehl, A., Sulzer, P., Fehrenbacher, D., Rybka, T., Seletskiy, D. V. & Leitenstorfer, A. Deterministic Nonlinear Transformations of Phase Noise in Quantum-Limited Frequency Combs. *Physical Review Letters* **122,** 203902 (2019).

50. Yu, S.-P., Cole, D. C., Jung, H., Moille, G. T., Srinivasan, K. & Papp, S. B. Spontaneous Pulse Formation in Edgeless Photonic Crystal Resonators. *Nature Photonics* **15,** 461–467 (2021).

51. Ulanov, A. E., Wildi, T., Pavlov, N. G., Jost, J. D., Karpov, M. & Herr, T. Synthetic Reflection Self-Injection-Locked Microcombs. *Nature Photonics,* 1–6 (2024).

52. Xue, X., Xuan, Y., Wang, P.-H., Liu, Y., Leaird, D. E., Qi, M. & Weiner, A. M. Normal-Dispersion Microcombs Enabled by Controllable Mode Interactions. *Laser & Photonics Reviews* **9,** L23–L28 (2015).

53. Clark, K. A., Cletheroe, D., Gerard, T., Haller, I., Jozwik, K., Shi, K., Thomsen, B., Williams, H., Zervas, G., Ballani, H., Bayvel, P., Costa, P. & Liu, Z. Synchronous Subnanosecond Clock and Data Recovery for Optically Switched Data Centres Using Clock Phase Caching. *Nature Electronics* **3,** 426–433 (2020).

54. Xue, X. & Calabretta, N. Nanosecond Optical Switching and Control System for Data Center Networks. *Nature Communications* **13,** 2257 (2022).

55. Gonzalez, J., G. Palma, M., Hattink, M., Rubio-Noriega, R., Orosa, L., Mutlu, O., Bergman, K. & Azevedo, R. Optically Connected Memory for Disaggregated Data Centers. *Journal of Parallel and Distributed Computing* **163,** 300–312 (2022).

56. Clivati, C., Meda, A., Donadello, S., Virzì, S., Genovese, M., Levi, F., Mura, A., Pittaluga, M., Yuan, Z., Shields, A. J., Lucamarini, M., Degiovanni, I. P. & Calonico, D. Coherent Phase Transfer for Real-World Twin-Field Quantum Key Distribution. *Nature Communications* **13,** 157 (2022).

57. Wang, S., Yin, Z.-Q., He, D.-Y., Chen, W., Wang, R.-Q., Ye, P., Zhou, Y., Fan-Yuan, G.-J., Wang, F.-X., Chen, W., Zhu, Y.-G., Morozov, P. V., Divochiy, A. V., Zhou, Z., Guo, G.-C. & Han, Z.-F. Twin-Field Quantum Key Distribution over 830-Km Fibre. *Nature Photonics* **16,** 154–161 (2022).

58. Wang, Z., Li, K., Wang, Y., Zhou, X., Cheng, Y., Jing, B., Sun, F., Li, J., Li, Z., Wu, B., Gong, Q., He, Q., Li, B.-B. & Yang, Q.-F. Large-Scale Cluster Quantum Microcombs. *Light: Science & Applications* **14,** 164 (2025).

59. Jia, X., Zhai, C., Zhu, X., You, C., Cao, Y., Zhang, X., Zheng, Y., Fu, Z., Mao, J., Dai, T., Chang, L., Su, X., Gong, Q. & Wang, J. Continuous-Variable Multipartite Entanglement in an Integrated Microcomb. *Nature* **639,** 329–336 (2025).

60. Ruiz-Chamorro, A., Garcia-Callejo, A. & Fernandez, V. Low-Complexity Continuous-Variable Quantum Key Distribution with True Local Oscillator Using Pilot-Assisted Frequency Locking. *Scientific Reports* **14,** 10770 (2024).